Chinese Journal of Physics 66 (2020) 444–452

Contents lists available at ScienceDirect

Chinese Journal of Physics

journal homepage: www.elsevier.com/locate/cjph

Forecasting and analysis of nonlinear optical responses by tuning the thickness of a doped hollow cylindrical quantum dot

M. Kria[a], M. El-Yadri[a], N. Aghoutane[a], L.M. Pérez[b], D. Laroze[b], E. Feddi[a]

[a] Group of Optoelectronic of Semiconductors and Nanomaterials, ENSET, Mohammed V University in Rabat, Morocco
[b] Instituto de Alta Investigación, CEDENNA, Universidad de Tarapacá, Casilla 7 D, Arica, Chile

ARTICLE INFO

Keywords:
Core-shell quantum dots
Donor impurity
Temperature effect
Pressure effect
Optical absorption coefficient
Refractive index changes

ABSTRACT

In present work, we theoretically study both the linear and the nonlinear absorption coefficient and refractive index related to the 1s-1p transition of a donor impurity in an AlAs/GaAs cylindrical core-shell quantum dot. Computations were carried out within the effective mass approximation employing a variational approach. It has been observed that optical responses of the core-shell quantum dot can be sensitively varied by changing shell thickness, impurity position, temperature, and pressure. Moreover, the absorption spectra reveals a large blue shift for the narrow shell width. The understanding of the optical transitions between the ground state (1s) and the first excited state (1p) in the structure can be applied for desirable features in nonlinear optics.

1. Introduction

The physics of semiconductor quantum dots (QDs) has attracted growing attention in the last few decades, both from the theoretical point of view as well as their applications, much of which is devoted to the manufacture of optoelectronic devices such as solar cells [1–3], lasers [4], and so on. Today, with his novel architecture, the core-shell quantum dots (CSQDs) are attracting widespread interest in modern materials science and technology.

The prospect of the potential application of CSQDs has driven extensive efforts to control precisely the core size and the shell thickness of the QD because their optical and electronic properties depend on these parameters [5–7]. This dependence provides a tunable handle to the optical absorption and emission characteristics. The first studies of this kind of QD have been applied to CdSe/CdS and ZnS/CdS [8].

Introducing impurities directly into the lattices was the most significant technological enhancement in the development of new electronic devices based on the semiconductor heterostructures, allowing to apply in the engineer's needs [9]. In our previous work [7], the impurity energy states have been scarcely investigated from the theoretical point of view in a cylindrical CSQD. The result shows that the impurity binding energy exhibits another behavior, mainly in the case of the narrow shell thickness. Indeed, the binding energy tends toward 2D limit energy when the inner radius tends to the outer radius in the case of spherical symmetry, while it still increases as the shell thickness reduces in cylindrical one. These energies have been discussed in ref [10], taking into account the hydrostatic pressure and the temperature effects. The study shows a remarkable impact of these two factors.

The numerical calculation of the optical properties in the core-shell structures with cylindrical symmetry can be realized based on the numerical results applied to the nanowires system. So we can mention, for instance, some works dedicated to this issue. The optical response through the coefficients of intersubband optical absorption and refractive index change has been examined in

E-mail addresses: dlarozen@uta.cl (D. Laroze), e.feddi@um5s.net.ma (E. Feddi).

https://doi.org/10.1016/j.cjph.2020.05.016
Received 25 March 2020; Received in revised form 6 May 2020; Accepted 18 May 2020
Available online 07 June 2020
0577-9073/ © 2020 The Physical Society of the Republic of China (Taiwan). Published by Elsevier B.V. All rights reserved.

Ref. [11]. The authors have presented a detailed calculation of the charge carrier states in a GaAs/$Al_xGa_{1x}As$ axially symmetric double core-shell quantum wire (CSQW), discussing the effect of change in the characteristic in-plane dimensions of the structure. They have shown that the influence of the external probes leads to the shift of the characteristic maxima (minima) of these coefficients when they are given as a function of the incident radiation energy [12]. It is important to note that the optical properties of other exotic shapes have been investigated in some interesting works as those developed by Khordad et al. [13,14]. The authors analyzed the effects of temperature, pressure and spin-orbit interaction on the absorption coefficient and refractive index changes in wedge-shaped in a V-groove quantum wire. Other related works can also be found in Refs. [15,16].

The nonlinear optical properties of new core-shell GaN/$Al_{0.1}Ga_{0.9}N$ nanowires [17] are examined. A finite difference method in cylindrical coordinates is employed to solve the corresponding radial SchrÃ¶dinger equation in the effective mass approximation. We obtain that the magnitude of the intersubband transitions and the optical absorption coefficients have an essential dependence of the resonance wavelength on the relaxation time and the core radius, respectively.

In this manuscript, although we refer to our earlier works [7,10], the focus is completely different. This one aims to investigate the refractive index changes and intersubband optical absorption coefficients in a cylindrical CSQDs with infinite potential confinement. After this brief overview of CSQD importance, the description of our theoretical model is presented in Section 2. We run our calculations in the framework of the effective mass approximation using a variational method to obtain the eigenvalues. The numerical results and the discussions are provided in Section 3. Our conclusions are drawn in Section 4.

2. Details of calculations

2.1. Determination of the eigenvalues

To analyze the optical responses due to a donor impurity localized inside GaAs nano-shell, we build our model bears a close resemblance to the one proposed in our previous works [10]. The GaAs nano-shell is characterized, as can be seen in Fig. 1, by its thickness $L_w = b - a$, where a and b are, respectively, the inner and the outer radius and its height H, which is assumed to be quite long than b ($H > > b$). We suppose that a wide-band dielectric medium typically surrounds the CSQD with a vast gap. This structure can be represented by a hollow cylinder from where the charge carriers may be trapped entirely inside the shell region.

In the parabolic band and the effective mass approximations, the temperature and pressure-dependent Hamiltonian of the donor impurity can be cast in the form:

$$\hat{\mathcal{H}} = -\frac{\hbar^2}{2\,m_e^*(P,\,T)}\nabla_e^2 + V_w^e(r_e) - \frac{e^2}{\varepsilon(P,\,T)|\vec{r_e} - \vec{r_D}|} \tag{1}$$

where $m_e^*(P,\,T)$ and $\varepsilon(P,\,T)$ are, respectively, the temperature and pressure-dependent effective mass of the electron and the static dielectric constant given by the following relations [18,19]:

$$m_e^*(P,\,T) = m_0\left[1 + 7.51\left(\frac{2}{E_g(P,\,T)} + \frac{1}{E_g(P,\,T) + \Delta_0}\right)\right]^{-1} \tag{2}$$

and

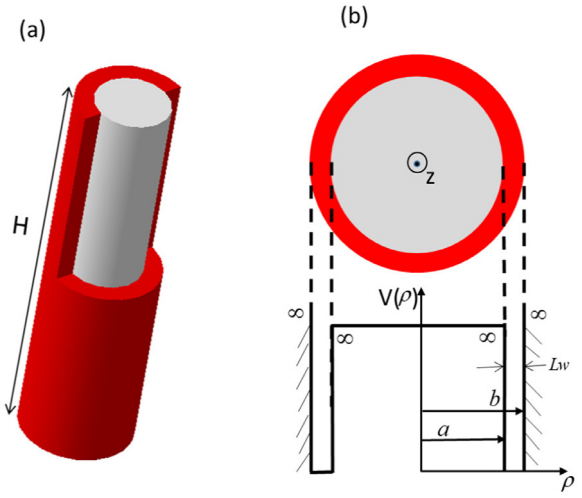


Fig. 1. (a) 3D-presentation of cylindrical core /shell QD. (b) The band diagram for radial confinement.

$$\varepsilon(P,\,T)=\begin{cases}12.7\exp(-1.67\times10^{-3}P)\exp(9.4\times10^{-5}(T-75.6)) & \text{for } 0\le T\le 200\,K\\ 13.18\exp(-1.73\times10^{-3}P)\exp(20.4\times10^{-5}(T-300)) & \text{for } T>200\,K\end{cases} \tag{3}$$

where $\Delta_0 = 0.341\ eV$ is the GaAs spin-orbit splitting, m_0 is the free electron mass, and $E_g(P,\,T)$ is the temperature and pressure-dependent GaAs bandgap at the center Γ of the Brillouin zone, and it can be written in terms of (meV) by the relation [18,20]:

$$E_g = 1.519 - \frac{5.4\times10^{-4}T^2}{T+204} + 0.01261P + 3.77\times10^{-5}P^2. \tag{4}$$

Let us note that in these relations, the temperature is in (K) and the pressure is expressed in ($kbar$). The notation $V_w^e(r_e)$ represents the quantum confinement potential. This potential can be expressed as the sum $V_w^e(r_e) = V_w^e(\rho_e) + V_w^e(z_e)$ due to the rigid barriers, such as:

$$V_w^e(\rho_e)=\begin{cases}0 & \text{for } a\le\rho_e\le b\\ \infty & \text{otherwise}\end{cases} \text{ and } V_w^e(z_e)=\begin{cases}0 & \text{for } |z_e|\le H/2\\ \infty & \text{for } |z_e|>H/2\end{cases} \tag{5}$$

By introducing the concept of the effective atomic units, we use the radius $a_D = \hbar^2\varepsilon/(m_e^* e^2)$ to express the length terms, and the Rydberg $R_D = \hbar^2/(2m_e^* a_D^2)$ to express terms of energy. Thus, Eq. (1) can be simplified to be:

$$\hat{\mathcal{H}} = -\frac{m_e^*}{m_e^*(P,\,T)}\left(\frac{\partial^2}{\partial\rho_e^2}+\frac{1}{\rho_e}\frac{\partial}{\partial\rho_e}+\frac{1}{\rho_e^2}\frac{\partial^2}{\partial\varphi_e^2}+\frac{\partial^2}{\partial z_e^2}\right)-\frac{\varepsilon}{\varepsilon(P,\,T)}\frac{2}{\sqrt{\rho_{eD}^2+(z_e-z_D)^2}}+V_1^e(\rho_e)+V_2^e(z_e) \tag{6}$$

where m_e^* and ε are taken at $P = 0\ kbar$ and $T = 300\ K$. Moreover, we note that $\rho_{eD} = \sqrt{\rho_e^2+\rho_D^2-2\rho_e\rho_D\cos(\varphi_e-\varphi_D)}$ is the xy-plane electron-impurity distance, z_e and z_D are the electron and impurity position along the z-direction, respectively. The eigenstates values of the considered system and the corresponding eigenfunctions Ψ_D^i can be determined by solving the famous Schrödinger equation:

$$\hat{\mathcal{H}}\Psi_D^j(\rho_e,\,\varphi_e,\,z_e) = E_D^j\,\Psi_D^j(\rho_e,\,\varphi_e,\,z_e) \tag{7}$$

$j = (1s,\,1p)$ designates the ground and the first state, respectively. The analytical solution seems to be impossible. Hence our choice as a resolution method is the variational approach using the following trial wave functions:

$$\Psi_D^j(\rho_e,\,\varphi_e,\,z_e) = N_j\,\Psi_e^j(\rho_e,\,\varphi_e,\,z_e)\rho_e^m\exp(-\alpha_j\rho_{eD})\exp(-\beta_j(z_e-z_D)^2) \tag{8}$$

with

$$\Psi_e^j(\rho_e,\,\varphi_e,\,z_e) = (A\,J_m(k_{mn}\rho_e)+B\,Y_m(k_{mn}\rho_e))\,e^{i\,m\,\varphi}\cos\left(\frac{\pi}{H}z_e\right) \tag{9}$$

where A and B are the normalization constants, J_m and Y_m are the m-order Bessel function ($m = 0$ for $1s$ and $m = 1$ for $1p$). k_{mn} represents the n^{th} root of the transcendental equation imposed by boundary conditions:

$$J_m(k_{mn}\,b)\,Y_m(k_{mn}\,a) - J_m(k_{mn}\,a)\,Y_m(k_{mn}\,b) = 0 \tag{10}$$

The two exponential terms in Eq. (8) reflect the Coulomb interaction between electron and impurity in the lateral and axial motion. The impurity total energy levels can be evaluated by minimizing the expected value of $\hat{\mathcal{H}}$ according to the following equation:

$$E_D^j = \min_{\alpha_j,\,\beta_j}\left\{\frac{<\Psi_D^j|\hat{\mathcal{H}}|\Psi_D^j>}{<\Psi_D^j|\Psi_D^j>}\right\} \tag{11}$$

with $j = (1s,\,1p)$.

2.2. Linear and third nonlinear optical properties

In the literature, $\alpha^{(1)}$ and $\alpha^{(3)}$ designate the linear and the third nonlinear photo-absorption coefficients (ACs), respectively. The mathematical formulation derived from the density matrix approach and perturbation theory. Thus we have [21–24]:

$$\alpha^{(1)}(\omega) = \omega\sqrt{\frac{\mu}{\varepsilon}}\frac{\hbar\,\Gamma\,|M_{\rm fi}|^2\,\sigma_s}{(E_{\rm fi}-\hbar\omega)^2+(\hbar\,\Gamma)^2} \tag{12}$$

and

$$\alpha^{(3)}(\omega,\,I) = -\omega\sqrt{\frac{\mu}{\varepsilon}}\left(\frac{I}{2\varepsilon_0 n_r c}\right)\frac{4\sigma_s\hbar\Gamma\,|M_{\rm fi}|^4}{[(E_{\rm fi}-\hbar\omega)^2+(\hbar\Gamma)^2]^2}\times\left[1-\frac{(M_{\rm ff}-M_{ii})^2}{4|M_{\rm fi}|^2}\left\{\frac{3E_{\rm fi}^2-4\hbar\omega E_{\rm fi}+\hbar^2(\omega^2-\Gamma^2)}{E_{\rm fi}^2+(\hbar\Gamma)^2}\right\}\right] \tag{13}$$

where $E_{\rm fi} = E_{\rm D}^{1p} - E_{\rm D}^{1s}$ denotes the difference between the first excited state energy and the ground state energy, $M_{\rm fi} = e < \Psi_D^{1p}|\vec{\rho}_{eD}.\,\hat{\varepsilon}|\Psi_D^{1s}>$ is the electric dipole moment of the transition from the $1s$ state to $1p$ state with $\hat{\varepsilon}$ is the unit polarization vector of the incident linearly polarized photon, and $\hbar\omega$ is the incident photon energy. The used parameters are: c for the speed of light in a vacuum, σ_s is the electron density related to the occupied volume by the relation, I is the intensity of the incident

electromagnetic radiation, μ is the permeability of the system, n_r is the relative refractive index of semiconductor, ε_0 is the vacuum permittivity, and Γ is the line width. Then the total absorption coefficient is defined:

$$\alpha(\omega, I) = \alpha^{(1)}(\omega) + \alpha^{(3)}(\omega, I) \tag{14}$$

It was found that the propagation of electromagnetic radiation through material produces changes also in the refractive index of this material. For this reason, we propose to study both linear and third-order nonlinear refractive index changes (RICs). In what follows, we write their expressions, respectively, as follows:

$$\frac{\Delta n^{(1)}(\omega)}{n_r} = \frac{1}{2\varepsilon_0 n_r^2}\frac{\sigma_s |M_{fi}|^2 (E_{fi} - \hbar\omega)}{(E_{fi} - \hbar\omega)^2 + (\hbar\Gamma)^2} \tag{15}$$

and

$$\frac{\Delta n^{(3)}(\omega, I)}{n_r} = -\frac{\mu c I \sigma_s |M_{fi}|^4}{\varepsilon_0 n_r^3}\frac{(E_{fi} - \hbar\omega)}{[(E_{fi} - \hbar\omega)^2 + (\hbar\Gamma)^2]^2} \times \left[1 - \frac{(M_{ff} - M_{ii})^2}{4|M_{fi}|^2(E_{fi}^2 + (\hbar\Gamma)^2)}\left\{E_{fi}(E_{fi} - \hbar\omega) - (\hbar\Gamma)^2 - (\hbar\Gamma)^2\frac{2(2E_{fi} - \hbar\omega)}{(E_{fi} - \hbar\omega)}\right\}\right] \tag{16}$$

Thus, the total RICs can be expressed as:

$$\frac{\Delta n(\omega)}{n_r} = \frac{\Delta n^{(1)}(\omega)}{n_r} + \frac{\Delta n^{(3)}(\omega)}{n_r} \tag{17}$$

3. Results and discussions

Numerical calculations on the linear and nonlinear optical responses were performed for cylindrical AlAs/GaAs CSQD, where the different parameters of GaAs material used for calculations at $P = 0\ Kbar$ and $T = 300\ K$ are listed in Table 1.

In the initial stage of the study, we would like to take a look at the impact of impurity position on the linear and third-order nonlinear optical responses. Following this, different photo-absorption coefficients and refractive index changes of a cylindrical AlAs/GaAs CSQD have been illustrated in Fig. 2 as a function of the incident photon energy. Three significant radial positions of impurity inside a typical core-shell sizes defined by $a = 0.5\ a_D$, $b = 1\ a_D$, and $H = 10\ a_D$ are considered: $\rho_D = (a + b)/2$, $\rho_D = a$, and $\rho_D = b$. As follows from Fig. 2, all curves present a significant peak at a specific energy value. It appears that the peak position strongly depends on the localization of the impurity inside the shell. The optical response occurs at higher photon energy in case of $\rho_D = (b + a)/2$ compared to two other cases $\rho_D = a$ and $\rho_D = b$. This apparent difference in the energy excitation threshold can be attributed to the behavior of electronic density around the ionized donor what will have an impact on the binding energy. Indeed, as we can see in Fig. 3, when the dopant is localized at the center of the shell ($\rho_D = (b + a)/2$), the system admits a high symmetrical localization of the electronic density around the ionized donor (Fig. 3a) which is explained by the maximum of the binding energy (Fig. 3d). While, when the impurity is placed at the borders of the well; $\rho_D = a$ and $\rho_D = b$; the symmetry is broken. Thus, the electronic densities are extended asymmetrically over all the well in the two extreme cases Fig. 3b and Fig. 3c In these cases, the binding energies have practically the lowest values as mentioned in Fig. 3d.

To understand the effect of the lateral size of the cylindrical nanostructure, defined by the radius (b), on the optical properties mainly in the two cases ($\rho_D = a$ and $\rho_D = b$), we clarified in Fig. 5, a comparison between the peak positions for the two considered donor positions. In this figure we present the optical properties for three different values of dot size b ($b = 1,\ 2$ and $3\ a_D$) while kipping the shell thickness constant ($L_w = b - a = 0.5\ a_D$). As we can see, in the case of small volume ($b = 1\ a_D$), which corresponds to strong confinement, a small difference between the peak positions relative to the two extreme locations of the impurity center. This is because of the double confinement imposed by the weakness of the dot size and the shrinking of the thickness L. In this case, the system becomes very sensitive to the position of the single dopant. However, this difference becomes more negligible and disappears for a large value of b, where the system behaves like a surface structure, and the confinement is considered as asymmetrical potential between the two rigid walls. In these cases, the densities are more spread along the lateral surface of the cylindrical quantum dot, and the system admits almost the same binding energy.

Let us first assume that the impurity is situated at the middle point of the shell ($\rho_D = (a + b)/2$ and $z_D = 0$), and incident light intensity is fixed at $I = 2{\cdot}10^4\ W/m^2$. We will consider examining the impact of the cylinder parameters. Panels (a) and (b) of Fig. 4a show the variation of linear, and the total AC and RI changes related to the transition $1s - 1p$ plotted versus the incident photon energy for a fixed outer radius b and three values of core radius $a = 1,\ 2$ and $3a_D$. The single dopant of impurity will be placed at the center of the shell $\rho_D = (a + b)/2$. We remark that because of the negative nonlinear terms, the peaks of total AC and RI are weakened

Table 1
Physical parameters of GaAs [18–20].

$m_e^* = 0.063\ m_0$	$\varepsilon = 13.18$
$E_g = 1.42\ eV$	$n_r = 3.2$
$a_D = 11.07\ nm$	$\sigma = 3.\ 10^{22}\ m^{-3}$
$R_D = 4.93\ meV$	$\Gamma_{fi} = 0.2\ ps^{-1}$

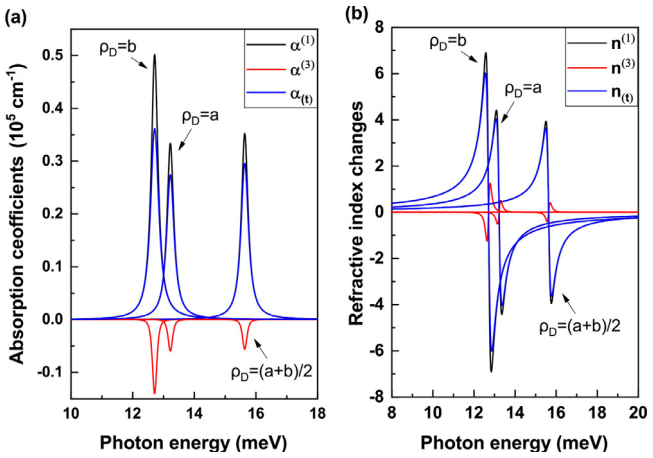


Fig. 2. Optical properties behavior ((a) ACs and (b) RICs) of a donor impurity system in an AlAs/GaAs CSQD as a function of the incident photon energy with three different impurity positions. The physical characteristics are taken at $T = 300\,K$ and P= $0\,Kbar$.

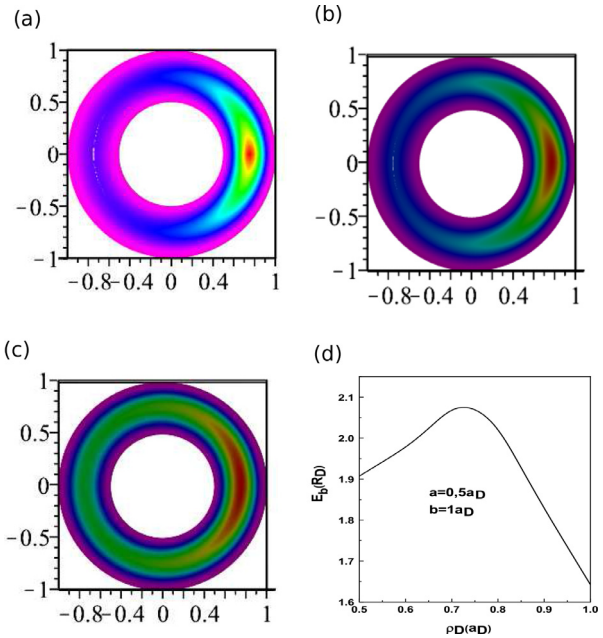


Fig. 3. Cross section of the radial probability density $\rho_D^2\Psi_D^2$ for the three significant ionized donor positions: $\rho_D = (a + b)/2$ (a), $\rho_D = a$ (b) and $\rho_D = b$ (c). In (d) we plot the variation of the binding energy as a function of the donor position ρ_D for $a = 0.5\,a_D$ and $b = 1\,a_D$..

compared to the linear response. The shift to high energies when decreasing the thickness of the shell can be interpreted using Eqs. (13) to (17). Indeed the Eqs. (15) and (16) show that RI vanishes when $\hbar\omega$ tends to the transition energy E_{fi} while AC reaches a maximum as seen in Eqs. (12) and (13). The increasing transition energy E_{fi} with the confinement effect explains the displacement of all curves towards higher energies. Another point to underline is that the decrease of the AC and RI amplitudes is due to the weakening of the intensity of the electric dipole matrix element M_{fi} when one goes to the low confinement regime.

These variations have been illustrated in Fig. 6 from which it can be seen that the peak position shifts inversely proportional to the shell volume. The difference appears on threshold energy value, which depends heavily on the values of b and a. It can suit the engineers needed. The peak values of the ACs and RICs with a fixed core radius $a = 1\,a_D$ and the outer radius of the shell $b = 2,\ 3$ and $4\,a_D$.

Fig. 7 shows the plot of the linear and the third-order nonlinear optical ACs and RICs as a function of incident photon energy for three different values of inner radius a and outer radius b with the same thickness $L_w = 1\,a_D$. As a first remark, the threshold energy tends to higher energy when the whole core-shell dot sizes are reduced. The illustrated curves in Fig. 7 serve to clarify that the optical responses do not explicitly depend only on the shell thickness (L_w) but depend in fact on the shell volume $V = \pi.\ H(b^2 - a^2)$. As the volume augments, the optical responses appear in the region of lower energies (red-shift).

In the next, the impact of the temperature and hydrostatic pressure is discussed. We recall that in our previous paper [10], we

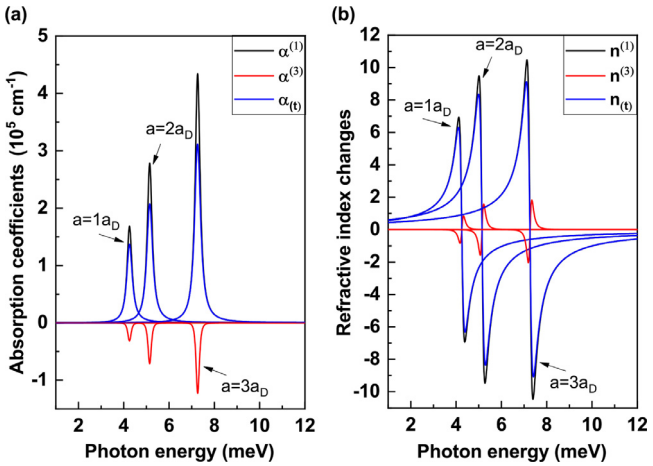


Fig. 4. Optical properties comportment ((a) ACs and (b) RICs) of a donor impurity system in an AlAs/GaAs cylindrical CSQD quantum dot in line with the incident photon for energy different values of the inner radius a at fixed outer radius $b = 4\ a_D$. The impurity assumed to be at the shell medium $\rho_D = (a + b)/2$ and the condition of T and P taken as $T = 300\,K$ and P= $0\,Kbar$.

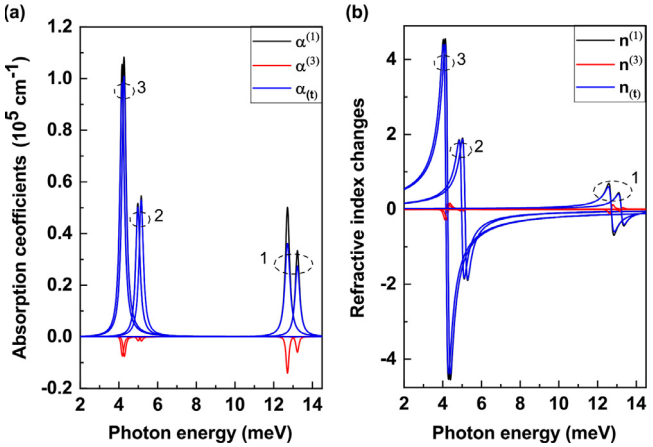


Fig. 5. Optical properties response ((a) ACs and (b) RICs) of a donor impurity system in an AlAs/GaAs cylindrical CSQD as a function of the incident photon energy for two typical impurity positions $\rho_D = a$ and $\rho_D = b$. The curves tend to clarify the threshold energy shift between the two considered impurity positions with the same shell thickness $L_w = 0.5\ a_D$, and for three different cases: case 1 ($a = 0.5\ a_D$ and $b = 1\ a_D$), case 2 ($a = 1.5\ a_D$ and $b = 2\ a_D$), and case 3 ($a = 2.5\ a_D$ and $b = 3\ a_D$). In each case, the left resonance peak refers to the impurity position ($\rho_D = a$) and the right one to ($\rho_D = b$). A symmetry is achieved for a large core volume.

have detailed the behavior of the binding energy as a function of the temperature and pressure. We have demonstrated that these two external perturbations have a significant antagonist influences on the impurity binding energy for large shell quantum dot. The electron-ionized donor interaction is more pronounced with increasing pressure and decreasing temperature for any impurity position and quantum dot size. In Fig. 8, the pressure effect on both Optical ACs and RICs is remarkable. The increases of the applied pressure promote the shell material to absorb in the region of higher energy, which points to the usefulness of pressure as a seat of additive quantum confinement without changing the size of the (CSQD). This effect was expected because an applied hydrostatic pressure tends to exert a stress on the rearrangement of atoms in a way to reduce the mesh of the crystal, which reinforces the electron-impurity interaction. Therefore the shell will need to absorb sufficient energy to favor the impurity transition from the ground state to the excited one. Furthermore, the absorption coefficient is more pronounced for low pressure than the high pressure, and this is due to the augmentation of the optical integral M_{fi} when the pressure is increased.

We remark that the effect of the temperature on the optical properties produces the inverse effect of the pressure. Fig. 9 depicts the donor impurity related optical ACs and RICs for different values of temperature as a function of the incident photon energy. The temperature strongly determines the value of the linear and the third-order nonlinear optical absorption coefficients and refractive index in the resonance peak, which is increased with temperature. We also note a slight variation of the threshold energy to the small incident photon energy. The reason is because of the transition energy E_{fi} decreases as the temperature increases in the range of (100, 300) K. Taken into consideration the study that has been done on the hydrostatic pressure and the temperature effect on a single dopant in cylindrical CSQD [10], we can resume that the optical ACs and RICs coefficients follow the same behavior of impurity

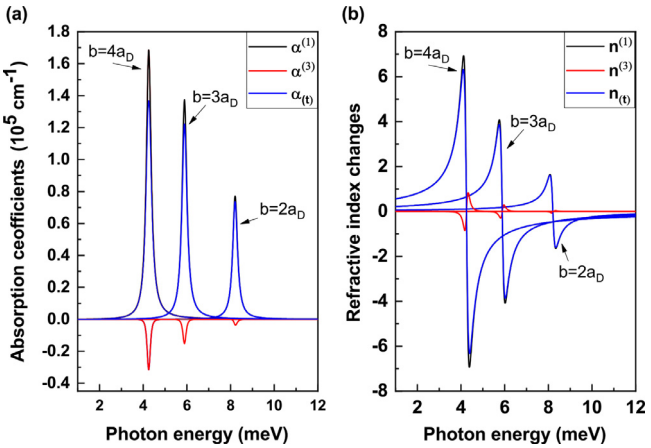


Fig. 6. Optical properties behavior ((a) ACs and (b) RICs) of a donor impurity system in a AlAs/GaAs cylindrical CSQD as a function of the incident photon energy for a different values of the outer radius b at fixed core radius $a = 1\,a_D$. The impurity is localized at the shell medium with ($\rho_D = (a + b)/2$ and $z_D = 0$) and the system supposed to be at $T = 300\,K$ and P= 0 $Kbar$.

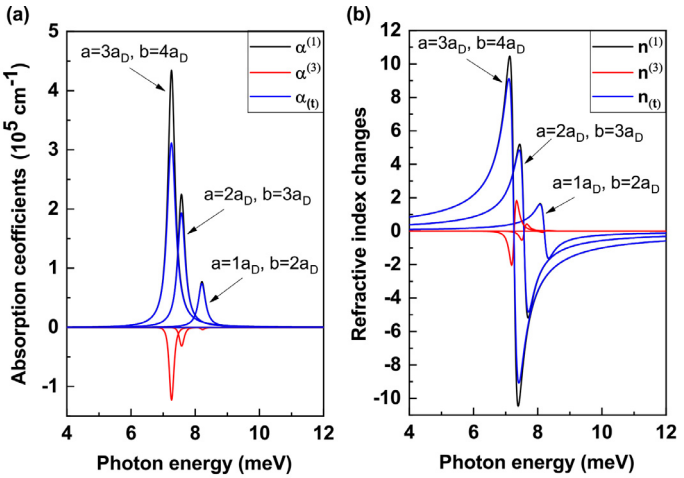


Fig. 7. Optical properties analysis ((a) ACs and (b) RICs) of a donor impurity system in a AlAs/GaAs cylindrical CSQD as a function of the incident photon energy for a fixed shell thickness $b - a = 1\,a_D$. The impurity is localized at the shell medium with ($\rho_D = (a + b)/2$ and $z_D = 0$), the temperature $T = 300\,K$, and the pressure P= 0 $Kbar$.

energy eigenvalue.

4. Conclusions

In conclusion, our work has treated the impact of the cylindrical core-shell quantum dots sizes, the impurity positions, the temperature on the linear and third-order nonlinear optical properties, and the hydrostatic pressure. The evidence from this study implies that the optical responses depend strongly on all these parameters either to induce them to be exited at low energies or the highest energies. We plan to extrapolate this study to consider a finite barrier potential. This general case must take into account the relative alignment of the energy bands (band offset) of the two materials, which could lead to Type I or type II core /shell structures. In these compelling cases, several phenomena are to be taken into account, especially the phenomena of polarization and dielectric mismatch. Nonetheless, we are confident that our results may improve knowledge about optoelectronic properties in hollow cylindrical core-shell quantum dots, as well as a useful aid for optoelectronic devices.

Declaration of Competing Interest

The authors declare that they have no conflict of interest.

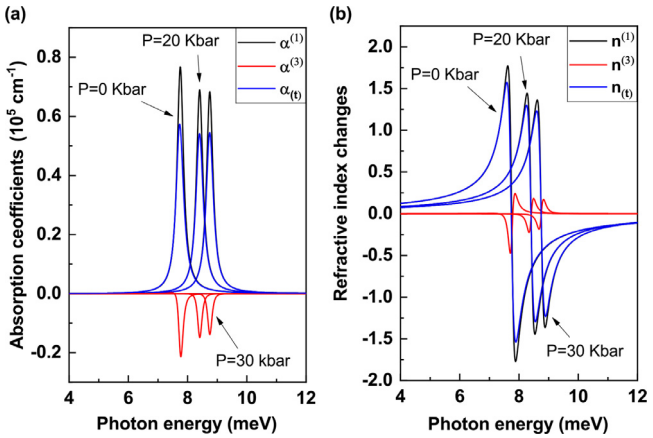


Fig. 8. Optical properties behavior ((a) ACs and (b) RICs) of a donor impurity system in a AlAs/GaAs cylindrical CSQD as a function of the incident photon energy under the influence of pressure P. The impurity is sited at the shell medium with ($\rho_D = (a + b)/2$ and $z_D = 0$), the temperature fixed at $T = 300\,K$.

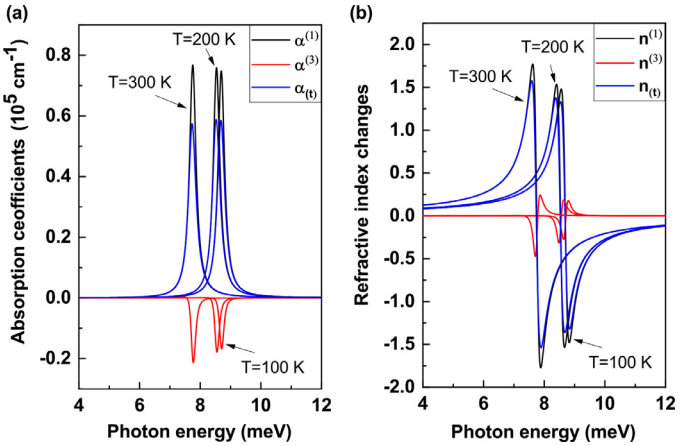


Fig. 9. Optical properties variation ((a) ACs and (b) RICs) of a donor impurity system in a AlAs/GaAs cylindrical CSQD as a function of the incident photon energy under the influence of temperature T. The impurity is localized at the shell medium with ($\rho_D = (a + b)/2$ and $z_D = 0$) and by considering the zero applied pressure.

Acknowledgments

LMP and DL acknowledge partial financial support from FONDECYT 1180905. DL acknowledges partial financial support from Centers of excellence with BASAL/CONICYT financing, Grant AFB180001, CEDENNA.

References

[1] X. Zhang, C.W. Pinion, J.D. Christesen, C.J. Flynn, T.A. Celano, J.F. Cahoon, Horizontal silicon nanowires with radial p–n junctions: a platform for unconventional solar cells, J. Phys. Chem. Lett. 4 (12) (2013) 2002–2009.
[2] J.J. Wierer Jr, Q. Li, D.D. Koleske, S.R. Lee, G.T. Wang, III-Nitride core–shell nanowire arrayed solar cells, Nanotechnology 23 (19) (2012) 194007.
[3] L. Dupré, D. Buttard, P. Gentile, N. Pauc, A. Solanki, High density core-shell silicon nanowire array for the realization of third generation solar cell, Energy Procedia 10 (2011) 33–37.
[4] F. Qian, Y. Li, S. Gradečak, H.-G. Park, Y. Dong, Y. Ding, Z.L. Wang, C.M. Lieber, Multi-quantum-well nanowire heterostructures for wavelength-controlled lasers, Nat. Mater. 7 (9) (2008) 701.
[5] N. Aghoutane, M. El-Yadri, A. El Aouami, E. Feddi, G. Long, M. Sadoqi, F. Dujardin, C.V. Nguyen, N.N. Hieu, H.V. Phuc, Excitonic nonlinear optical properties in AlN/GaN spherical core/shell quantum dots under pressure, MRS Commun. 222 (2019) 1–7.
[6] A. Talbi, E. Feddi, A. Zouitine, M. El Haouari, M. Zazoui, A. Oukerroum, F. Dujardin, E. Assaid, M. Addou, Control of the binding energy by tuning the single dopant position, magnetic field strength and shell thickness in ZnS/CdSe core/shell quantum dot, Physica E 84 (2016) 303–309.
[7] E. Feddi, M. El-Yadri, F. Dujardin, R. Restrepo, C. Duque, Photoionization cross section and binding energy of single dopant in hollow cylindrical core/shell quantum dot, J. Appl. Phys. 121 (6) (2017) 064303.
[8] S. Mathew, A.D. Saran, B. Singh Bhardwaj, S. Ani Joseph, P. Radhakrishnan, V. Nampoori, C. Vallabhan, J.R. Bellare, Size dependent optical properties of the CdSe − CdS core-shell quantum dots in the strong confinement regime, J. Appl. Phys. 111 (7) (2012) 074312.
[9] P. Harrison, A. Valavanis, Quantum Wells, Wires and Dots: Theoretical and Computational Physics of Semiconductor Nanostructures, John Wiley & Sons, 2016.
[10] M. El-Yadri, N. Aghoutane, A. El Aouami, E. Feddi, F. Dujardin, C. Duque, Temperature and hydrostatic pressure effects on single dopant states in hollow

cylindrical core-shell quantum dot, Appl. Surf. Sci. 441 (2018) 204–209.
[11] G.L. Miranda, M.E. Mora-Ramos, C.A. Duque, Exciton-related nonlinear optical absorption and refractive index change in GaAs–$Ga_{1-x}Al_xAs$ double quantum wells, Physica B 409 (2013) 78–82.
[12] C. Duque, M. Mora-Ramos, C. Duque, Carrier states and optical response in core–shell-like semiconductor nanostructures, Philos. Mag. 97 (5) (2017) 368–388.
[13] R. Khordad, B. Vaseghi, Effects temperature, pressure and spin–orbit interaction simultaneously on third harmonic generation of wedge-shaped quantum dots, Chin. J. Phys. 59 (2019) 473–480.
[14] R. Khordad, S.K. Khaneghah, M. Masoumi, Effect of pressure on intersubband optical absorption coefficients and refractive index changes in a v-groove quantum wire, Superlattices Microstruct. 47 (2010) 538–549.
[15] R. Khordad, Simultaneous effects of temperature and pressure on the donor binding energy in a v-groove quantum wire, Superlattices Microstruct. 47 (2010) 422–431.
[16] R. Khordad, H. Bahramiyan, H.R. Rastegar Sedehi, Effects of strain, magnetic field and temperature on entropy of a two dimensional gaas quantum dot under spin-orbit interaction, Opt. Quantum Electron. 50 (2018) 294.
[17] M. Kouhi, Nonlinear optical absorption in the core shell nanowire, Int. J. Mod. Phys. B 31 (23) (2017) 1750164.
[18] Z. Zeng, G. Gorgolis, C.S. Garoufalis, S. Baskoutas, Competition effects of electric and magnetic fields on impurity binding energy in a disc-shaped quantum dot in the presence of pressure and temperature, Sci. Adv. Mater. 6 (3) (2014) 586–591.
[19] S. López, N. Porras-Montenegro, C. Duque, Excitons in coupled quantum dots: hydrostatic pressure and electric field effects, Physica Status Solidi (b) 246 (3) (2009) 630–634.
[20] C. Duque, S. López, M. Mora-Ramos, Basic solid state physics, Phys. Stat. Sol.(b) 244 (6) (2007) 1964–1970.
[21] W. Xie, Impurity effects on optical property of a spherical quantum dot in the presence of an electric field, Physica B 405 (16) (2010) 3436–3440.
[22] M. Vahdani, G. Rezaei, Linear and nonlinear optical properties of a hydrogenic donor in lens-shaped quantum dots, Phys. Lett. A 373 (34) (2009) 3079–3084.
[23] A. Jafari, Optical properties of hydrogenic impurity in an inhomogeneous infinite spherical quantum dot, Physica B 456 (2015) 72–77.
[24] M. Abramowitz, I. Stegun, (1970): (Handbook of Mathematical Functions, (Dover Publications, Inc., (New York.